

Dark spot, Spiral waves and the SW Sex behaviour: it is all about UX Ursae Majoris

V. V. Neustroev^{1*}, V. F. Suleimanov^{2,3}, N. V. Borisov⁴, K. V. Belyakov³, and A. Shearer¹

¹Centre for Astronomy, National University of Ireland, Galway, Newcastle Rd., Galway, Ireland

²Institute for Astronomy and Astrophysics, Kepler Center for Astro and Particle Physics, Eberhard Karls University, Sand 1, 72076 Tübingen, Germany

³Kazan State University, Kremlevskaja str. 18, Kazan 420008, Russia

⁴Special Astrophysical Observatory of the Russian AS, Nizhnij Arkhyz, Karachaev-Cherkesia 369167, Russia

Accepted ????. Received ????. in original form 2009 December 7

ABSTRACT

We present an analysis of time-resolved, medium resolution optical spectroscopic observations of UX UMa in the blue (3920–5250 Å) and red (6100–7200 Å) wavelength ranges, that were obtained in April 1999 and March 2008 respectively. The observed characteristics of our spectra indicate that UX UMa has been in different states during those observations. The blue spectra are very complex. They are dominated by strong and broad single-peaked emission lines of hydrogen. The high-excitation lines of He II $\lambda 4686$ and the Bowen blend are quite strong as well. All the lines consist of a mixture of absorption and emission components. Using Doppler tomography we have identified four distinct components of the system: the accretion disc, the secondary star, the bright spot from the gas stream/disc impact region, and the unique compact area of absorption in the accretion disc seen as a dark spot in the lower-left quadrant of the tomograms. In the red wavelength range, both the hydrogen (H α) and neutral helium (He I $\lambda 6678$ and He I $\lambda 7065$) lines were observed in emission and both exhibited double-peaked profiles. Doppler tomography of these lines reveals spiral structure in the accretion disc, but in contrast to the blue wavelength range, there is no evidence for either the dark spot or the gas stream/disc impact region emission, while the emission from the secondary star is weak. During the observations in 1999, UX UMa showed many of the defining properties of the SW Sex stars. However, all these features almost completely disappeared in 2008. We have also estimated the radial velocity semi-amplitudes K_1 and K_2 and evaluated the system parameters of UX UMa. These estimates are inconsistent with previous values derived by means of analysis of WD eclipse features in the light curve in the different wavelength ranges.

Key words: methods: observational – accretion, accretion discs – binaries: close – novae, cataclysmic variables – stars: individual: UX UMa

1 INTRODUCTION

Cataclysmic Variables (CVs) are close interacting binaries that contain a white dwarf (WD) accreting material from a companion, usually a late main-sequence star. CVs are very active photometrically, exhibiting variability on time scales from seconds to centuries (see Warner 1995 for a general review on CVs).

Nova-like variables (NLs) are an important subset of CVs. By definition, NLs should not display any dwarf nova (DN) outbursts. Their almost steady brightness is thought to be due to their mass transfer rate \dot{M} exceeding the upper stability limit \dot{M}_{crit} . Their discs are thus thermally and tidally stable. As a consequence of such a nebulous definition, the NL class is a very heteroge-

neous group of stars, and the definition of the subclasses within NLs is mostly based on observational features of objects. According to Warner (1995), the UX Ursae Majoris stars show persistent broad Balmer absorption lines, and this terminology has occasionally been used for all NLs. The RW Triangulum stars, per contra, have pure emission-line spectra. A significant fraction of NLs show states of low luminosity in their long-term optical light curves at irregular intervals of weeks to months. Those of them having drops exceeding 1 mag are known as the “anti-dwarf novae” or VY Sculptoris stars (La Dous 1993; Warner 1995; Dhillon 1996).

SW Sextantis stars are another relatively large group of NLs, which was initially populated by eclipsing systems only (Thorstensen et al. 1991). These systems, largely occupying the narrow orbital period stripe between 3 and 4.5 hours, show many unusual yet consistent properties, including single-peaked emission

* E-mail: vitaly@neustroev.net

lines despite the high inclination, strong high excitation spectral features, central absorption dips in the emission lines around phase 0.4 – 0.7, and high-velocity emission S-waves with maximum blueshift near phase ~ 0.5 . The unusual spectroscopic behaviour of the SW Sex systems has led to their intensive studies and many NLs above the 3 – 4.5 hr period interval, and even some Low Mass X-ray Binaries (LMXBs) have been found to exhibit distinctive SW Sex behaviour¹ (Rodríguez-Gil, Schmidtobreick, Gänsicke 2007; Rodríguez-Gil et al. 2007).

In this paper we report on our observations of UX UMa, a prototype of the NLs, and show that this system also exhibits some of the key features of the SW Sex stars. UX UMa has been discovered by Beljavsky (1933) and extensively studied in the past (Walker & Herbig 1954; Warner & Nather 1972), and is considered to be one of the well known CVs. UX UMa has an orbital period of 4.72 h (Kukarkin 1977) and is the brightest eclipsing NL. Warner & Nather (1972) found low-amplitude 29-s oscillations in the light curve of UX UMa confirmed later by Knigge et al. (1998). It could be interpreted in the context of a low-inertia magnetic accretor, in which accretion on to an equatorial belt of the WD primary causes the belt to vary its angular velocity (Warner & Woudt 2002). Rutten et al. (1993, 1994) presented spectrally-resolved eclipse maps of the UX UMa accretion disc, obtained from low-resolution spectra spanning $\lambda\lambda 3600\text{--}9800 \text{ \AA}$. The system has been also well studied in ultraviolet (Baptista et al. 1995; Knigge et al. 1998; Froning, Long, & Knigge 2003; Linnell et al. 2008) and X-rays (Wood, Naylor, & Marsh 1995; Pratt et al. 2004) in recent years. The system parameters for UX UMa are usually taken from Baptista et al. (1995) and are based on the derived parameters of a WD eclipse, which however has been brought into question by Froning, Long, & Knigge (2003).

Despite such a rich history of investigations, UX UMa has been almost neglected with optical high or medium resolution spectroscopy for the past 25 years. To our knowledge, no detailed red spectra of UX UMa have been published at all, with the exception of several profiles of the H α emission line (Kjurkchieva et al. 2006), and the far-red spectra in the wavelength range $\lambda\lambda 7661\text{--}8308 \text{ \AA}$ (Vande Putte et al. 2003). The latest extensive optical spectroscopic studies of this system in the blue wavelength range have been made by Schlegel, Honeycutt, & Kaitchuck (1983). In particular, they found that the optical lines exhibited a wide range of radial velocity semi-amplitudes, varying from line to line. Soon after Shafter (1984) found K_1 for H α equal $157 \pm 6 \text{ km s}^{-1}$. This value of the semi-amplitude implies a mass ratio of $q = 1$, making UX UMa one of the few systems where the masses of the primary and secondary stars are the same (Baptista et al. 1995). Nevertheless, Vande Putte et al. (2003) estimated K_2 to be 262 ± 14 , whereas Froning, Long, & Knigge (2003) found the extremely low K_1 of 70 km s^{-1} for far ultraviolet absorption lines. Suleimanov et al. (2004) gave a preliminary analysis on part of the data presented in this paper, and estimated the semi-amplitude of the radial-velocity variations of the H β emission line to be about 100 km s^{-1} . They also found that UX UMa showed some features which are commonly used for the identification of the SW Sex subclass stars.

This motivated us to perform a new time-resolved spectroscopy of UX UMa in order to study its properties in more detail.

In this paper we present and discuss the medium-resolution spectroscopic observations of the system in 1999 and 2008.

2 OBSERVATIONS AND DATA REDUCTION

The spectra presented here were obtained during two observing runs. The first observations were conducted in 1999 during two nights of April 8 and 10 at the Special Astrophysical Observatory of the Russian Academy of Sciences (SAO RAS) on the 6 m telescope, using the UAGS spectrograph, equipped with a Photometrics CCD. A total of 62 spectra in the wavelength range of $3920\text{--}5250 \text{ \AA}$ and a dispersion of $\sim 1.3 \text{ \AA/pix}$ were obtained with 300 s individual exposures. Corresponding spectral resolution was about 2.5 \AA .

Further observations were obtained in 2008 during 3 nights of March 20, 22 and 24, using the imaging spectrograph BFOSC with a 1300×1340 pixels EEV CCD attached to the Cassini 1.5 m telescope at Loiano (Italy). Grism #8 was used, providing nominal spectral coverage of $6100\text{--}8190 \text{ \AA}$ and a dispersion of $\sim 1.6 \text{ \AA/pix}$. A total of 37 spectra were obtained with 600 s individual exposures. Corresponding spectral resolution was about 3.3 \AA .

The reduction procedure was performed using the MIDAS (the SAO observations) and IRAF (Loiano) environments. Comparison spectra of Ar-Ne-He (SAO) and He-Ar (Loiano) lamps were used for the wavelength calibration. The absolute flux calibration of the spectra was also achieved by taking nightly spectra of the standard stars BD+33 2642 (SAO), Feige 92 and Hiltner 600 (Loiano). However, as the weather conditions during both observing sets were not optimal due to cirrus and poor seeing (down to $3''$), we consider the flux calibration to be only approximate. In view of this fact, from now on we use spectra normalized to the continuum.

To improve the confidence of the results presented in this paper we also acquired the phase-binned spectra. For this the spectra were phase-folded according to the linear ephemeris of Baptista et al. (1995):

$$T_{min}(HJD) = 2443904.87872(\pm 3) + 0.196671278(\pm 2) \times E, \quad (1)$$

where T_{min} is the moment of minimum, and then co-added the spectra into 17 (SAO) and 24 (Loiano) separate phase bins.

The uncertainties of this ephemeris in orbital phase at the time of our observations are very small. For the Loiano observations, for which the propagated error is larger, it is less than 0.001. This is much smaller than our phase resolution (~ 0.035) and is thus negligible.

3 DATA ANALYSIS AND RESULTS

3.1 Averaged and trailed spectra

Optical spectra of NLs show a wide range of appearances. According to Warner (1995), the UX UMa stars have persistently broad Balmer absorption-line spectra, whereas the RW Tri stars, for example, have pure emission-line spectra (even though occasionally with absorption cores). It is interesting to note, however, that such segregation is quite vague, as even UX UMa itself does not exactly follow this definition.

The mean spectra of UX UMa in the blue wavelength range, from the SAO dataset, are shown in Fig. 1 (top panel). These spectra are an average and a combination of spectra in three phase intervals, uncorrected for orbital motion.

The spectra are dominated by strong and broad emission lines of hydrogen. The high-excitation lines of He II $\lambda 4686$ and the

¹ See D. W. Hoard's Big List of SW Sextantis Stars at <http://web.ipac.caltech.edu/staff/hoard/cvtools/swsex/biglist.html> (Hoard et al. 2003).

Table 1. Log of observations of UX UMa

Set	Date	HJD Start 2450000+	Instrument	$\Delta\lambda^a$ (Å)	λ range (Å)	Exp. Time (sec)	Number of exps.	Duration (hours)
SAO	1999-Apr-08	1277.384	UAGS	2.5	3920–5220	300	9	0.73
	1999-Apr-08	1277.504	UAGS	2.5	3920–5220	300	19	1.66
	1999-Apr-10	1279.324	UAGS	2.5	3920–5220	300	34	3.25
Loiano	2008-Mar-20	4546.521	BFOSC	3.3	6100–8100	600	15	2.56
	2008-Mar-22	4548.453	BFOSC	3.3	6100–8100	600	7	1.16
	2008-Mar-24	4550.331	BFOSC	3.3	6100–8100	600	15	2.57

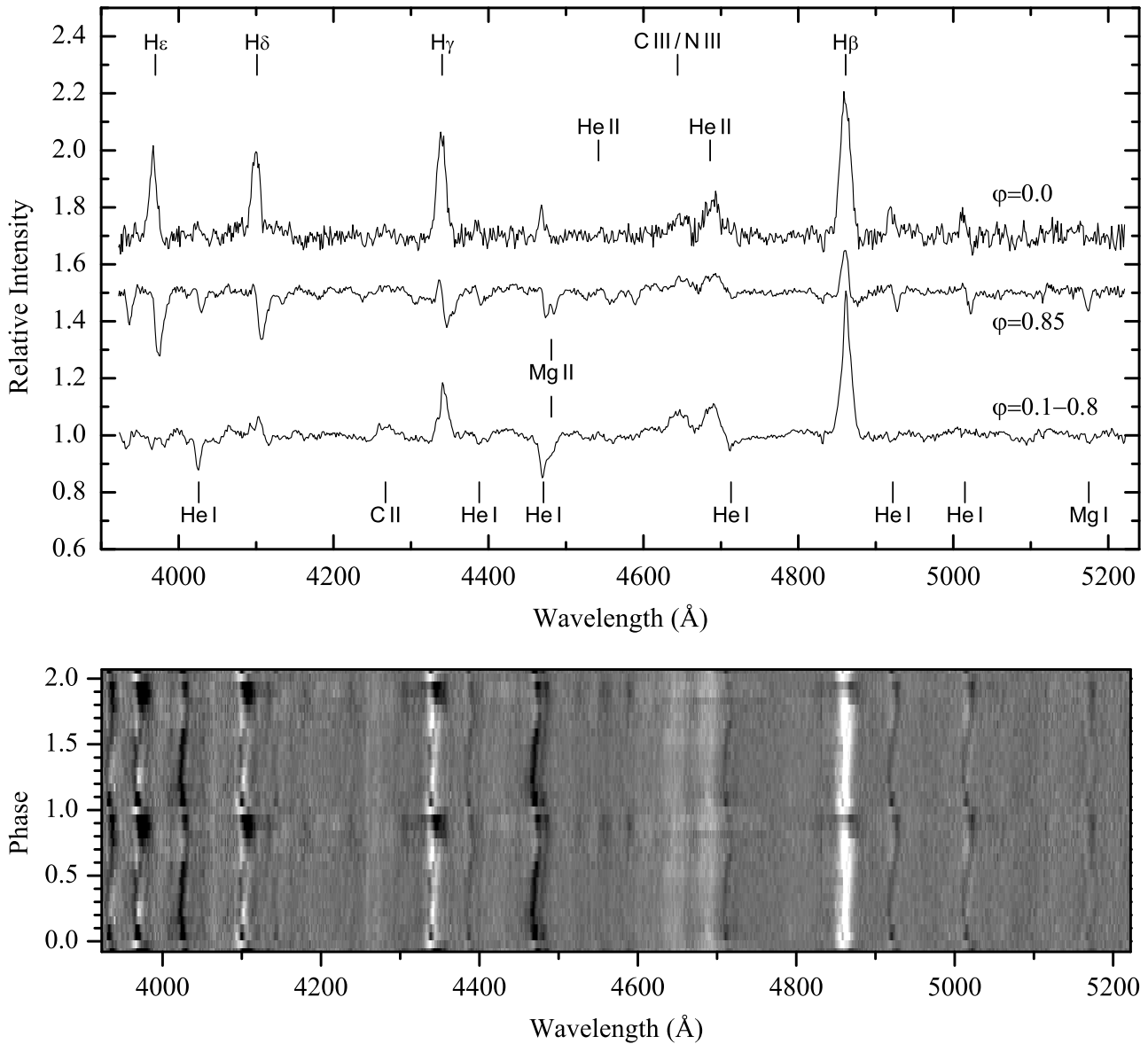
^a – $\Delta\lambda$ is the FWHM spectral resolution

Figure 1. Average (top panel) and trailed (bottom panel) spectra of UX UMa from the SAO set. The average spectrum is divided in three phase intervals. The top curve shows the spectrum in mid-eclipse ($0.025 < \varphi < 0.975$), the bottom curve shows the spectrum outside eclipse ($0.08 < \varphi < 0.78$), and the middle curve shows the spectrum outside but just prior to eclipse ($0.78 < \varphi < 0.92$). In the trailed spectrum, displayed twice for clarity, numerous emission and absorption features are visible. Note, that all the lines consist of a mixture of absorption and emission components. White indicates emission.

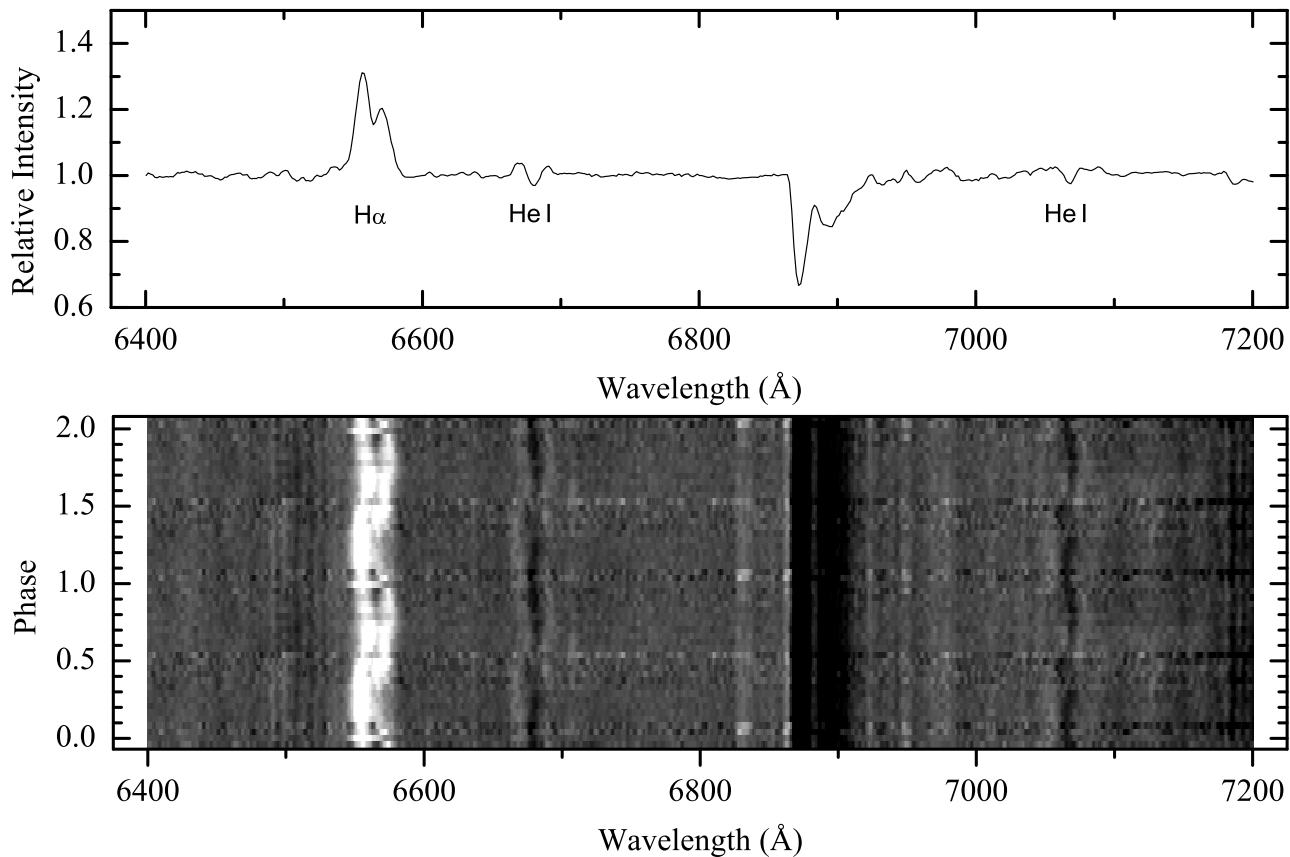


Figure 2. The red average (top panel) and trailed (bottom panel) spectra of UX UMa from the Loiano set.

C III/N III $\lambda 4640$ – 4650 blend are quite strong as well. In addition, He II $\lambda 4542$ and C II $\lambda 4267$ are observed. All these emission lines exhibit, in the averaged spectra, symmetric single-peaked profiles. However, in the phase-folded spectra the emission line-profile variations are quite complex and resemble those observed in SW Sex stars. For example, the Balmer lines H β and H γ are single-peaked but show transient absorption features at phases 0.4–0.7 turning the line profiles into the double-peak appearance (Fig. 3, left panel). The strength of this absorption increases with increasing line excitation level.

The absorption spectrum is also rich in features. In particular, we note that outside eclipse all the lines of neutral helium are in absorption, the strongest such features are He I $\lambda 4472$ and He I $\lambda 4026$. Also note the presence of the Mg I $\lambda 5175$ and Mg II $\lambda 4481$ absorption lines (Fig. 1, top panel, the bottom spectrum).

At phase $\varphi \sim 0.78$, a new absorption component appeared in the red wings of the Balmer emission lines and rapidly became so strong that it almost flooded the higher members of the Balmer lines (Fig. 1, top panel, the middle spectrum). However, this absorption apparently did not affect the high-excitation emission lines and very little distorted the He I absorption lines which in fact became less deep. There was little qualitative change in the eclipse spectrum of UX UMa before mid-eclipse ($0.025 < \varphi < 0.975$) when all absorptions were instantly reversed into emissions, and also the Balmer decrement became almost flat (Fig. 1, top panel, the upper spectrum).

Even more details can be found in the phase-resolved trailed spectra (Fig. 1, bottom panel). One can clearly recognize that the

phase 0.6 absorption mentioned before is in fact a manifestation of the sinusoidal absorption component of the emission lines seen continuously over the entire orbital period, which crosses from blue-shifted to red-shifted around phase ~ 0.6 . The semi-amplitude of its radial velocity variations can be roughly estimated to be $\sim 350 \text{ km s}^{-1}$, much more than published estimates of the radial velocity semi-amplitude of UX UMa’s WD. Thus, this absorption component with a nearly constant intensity originates somewhere on the far side of the accretion disc relative to the secondary star. Note also that all the lines including the deepest absorption lines He I $\lambda 4472$ and He I $\lambda 4026$, consist of a mixture of absorption and emission components. Thus, the difference in the appearance of the “emission” and “absorption” lines is determined mostly by the relative contributions of the corresponding components. Note that the absorption component of different lines seemingly varies in phase with each other. It is also interesting to mention that the broad absorption depression observed around the red wings of the lines just prior to eclipse, is certainly linked with those absorption components of the lines. From the trailed spectra of H β one can distinguish two sinusoidal emission components with different radial velocity amplitudes and phases. One of these components, with the smaller radial velocity amplitude, crosses from red-shifted to blue-shifted around phase ~ 0.5 and can probably be attributed to the secondary star (see also the trailed spectra in Fig. 6).

Surprisingly, the appearance and behaviour of the red spectrum was completely different from the spectrum in the blue wavelength range. Both the hydrogen (H α) and neutral helium (He I $\lambda 6678$ and He I $\lambda 7065$) lines were observed in emission and both

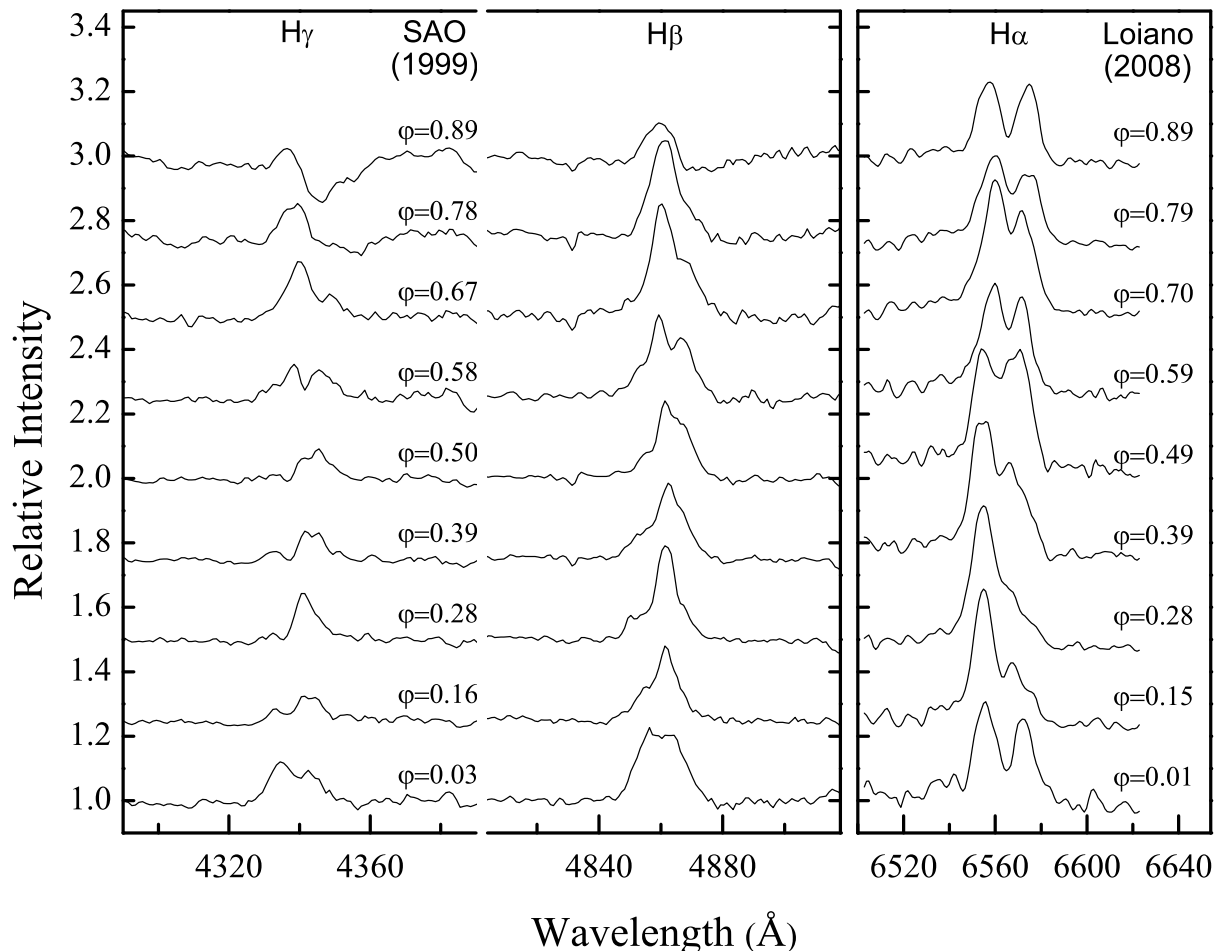


Figure 3. The line profile variations of UX UMa as a function of orbital phase. The left and right panels show the spectra from the SAO (1999) and Loiano (2008) observations respectively. The data have been averaged into 9 binary phase bins, and each resulting spectrum is normalized to the continuum and displaced along the intensity axis by 0.25.

exhibited double-peaked profiles though the depth of the central dip of the helium lines was below the continuum (Fig. 2). There was no visible change in the spectrum during the eclipse and neither high-velocity absorption nor emission appeared.

These clear changes between blue and red spectra may not be so surprising as these data sets are 9 years apart. On the other hand, care must be taken since we are not comparing the same wavelength ranges. Such differences between spectra can be due to different line transfer effects in different lines. We discuss this below.

3.2 Radial velocity study

A long standing problem in UX UMa is the measurement uncertainty of the radial velocity semi-amplitude of the WD. Obtaining an accurate value of K_1 has originally been one of the main aims of our time-resolved spectroscopy of UX UMa.

In CVs the most reliable parts of the emission line profile for deriving the radial velocity curve are the extreme wings. They are presumably formed in the inner parts of the accretion disc and therefore should represent the motion of the WD with the highest reliability. We measured the radial velocities using the double-Gaussian method described by Schneider & Young (1980) and later refined by Shafter (1983). This method consists of convolving each spectrum with a pair of Gaussians of width σ whose centres have a

separation of Δ . The position at which the intensities through the two Gaussians become equal is a measure of the wavelength of the emission line. The measured velocities will depend on the choice of σ and Δ , and by varying Δ different parts of the lines can be sampled. The width of the Gaussians σ is typically set by the resolution of the data.

The analysis of the trailed spectra (Section 3.1) and Doppler tomography (Section 4) shows that only few spectral lines can be used for radial velocity measurements using this method. Indeed, all the lines, with the exception of He II $\lambda 4686$ and C III / N III, consist of a mixture of absorption and emission components. The absorption component is very strong in most of the lines, especially in He I and the metal lines. It forms in a compact area of the accretion disc and its radial velocity curve does not reflect the orbital motion of the WD. This can be the reason for unrealistic values of the parameters of the radial velocity variations, obtained by Schlegel, Honeycutt, & Kaitchuck (1983) using “absorption” lines. However, this absorption component is much weaker in the Balmer lines and apparently does not affect their wings, except for the phases just prior to eclipse.

In order to test for consistency in the derived velocities and the zero phase, we separately used the emission lines H α and H β in the Loiano and SAO spectra respectively.

All the measurements were made using a Gaussian FWHM

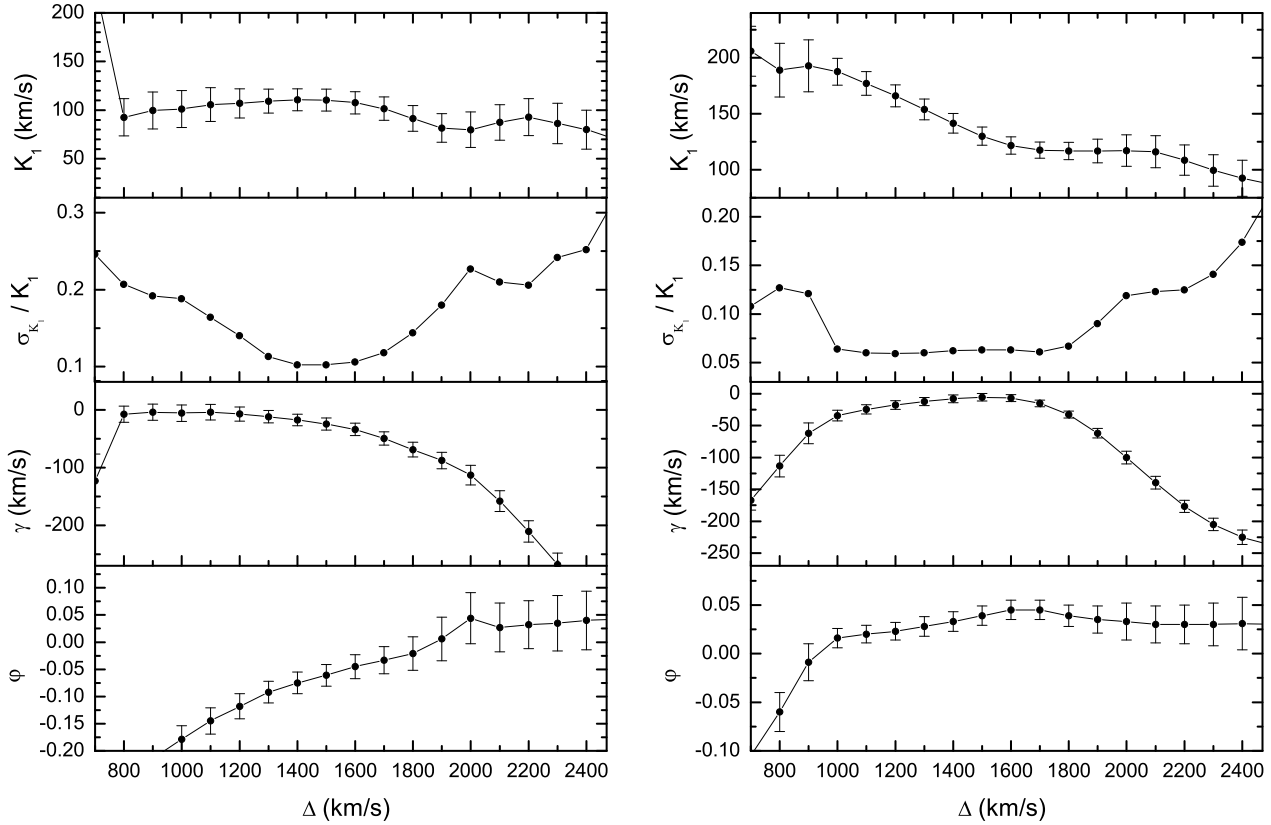


Figure 4. The diagnostic diagram for SAO’s $H\beta$ (left panel) and Loiano’s $H\alpha$ (right panel) data, showing the response of the fitted orbital elements to the choice of the double-gaussian separation. The best fit is reached with the gaussian separation of $1600\text{--}1700\text{ km s}^{-1}$ for $H\beta$ and 1800 km s^{-1} for $H\alpha$.

of 200 km s^{-1} and different values of the Gaussian separation Δ ranging from 300 km s^{-1} to 2500 km s^{-1} in steps of 100 km s^{-1} , following the technique of “diagnostic diagrams” (Shafter, Szkody, & Thorstensen 1986).

For each value of Δ we made a non-linear least-squares fit of the derived velocities to sinusoids of the form

$$V(\varphi, \Delta) = \gamma(\Delta) - K_1(\Delta) \sin[2\pi(\varphi - \varphi_0(\Delta))] \quad (2)$$

where γ is the systemic velocity, K_1 is the semi-amplitude, φ_0 is the phase of inferior conjunction of the secondary star and φ is the phase calculated according to the ephemeris (1). During this fitting procedure we omitted spectra covering the phase ranges $\varphi = \pm 0.08$, owing to measurement uncertainties during primary eclipse, and $\varphi = 0.78 - 0.92$, during which the red wing of $H\beta$ was affected by the absorption.

The resulting “diagnostic diagrams” are shown in Fig. 4. The diagrams show the variations of K_1 , $\sigma(K_1)/K_1$ (the fractional error in K_1), γ and φ_0 with Δ (Shafter, Szkody, & Thorstensen 1986). To derive the orbital elements of the line wings we took the values that correspond to the largest separation just before $\sigma(K_1)/K_1$ shows a sharp increase (Shafter & Szkody 1984). We find the maximum useful separation to be $\Delta_{max} \simeq 1800\text{ km s}^{-1}$ for $H\alpha$, and $\Delta_{max} \simeq 1600\text{ km s}^{-1}$ for $H\beta$. Note that K_1 is quite stable over a range of Gaussian separations around Δ_{max} , supporting their choice. One can see that K_1 for $H\alpha$ is practically constant for $\Delta > 1700\text{ km s}^{-1}$. For $H\beta$ K_1 is also very stable over a reasonable range in Δ of $1300\text{--}1600\text{ km s}^{-1}$ until the noise in the line wings begins to dominate.

We have obtained consistent results for both the radial velocity

semi-amplitudes and the γ -velocities for both lines. The measured parameters of the best fitting radial velocity curves are summarized in Table 2, whereas the radial velocity curves are shown in Fig. 5. The formal errors are the standard deviations determined during the least-square fits for the Gaussian separation Δ_{max} . They most likely underestimate the true errors, as they do not include a priori unknown systematic effects. A slightly non-sinusoidal shape of the curves can also alter the parameters. In the discussion to follow we adopt the value for K_1 to be $113 \pm 11\text{ km s}^{-1}$ which is the weighted mean for the $H\alpha$ and $H\beta$ lines (using $\sigma(K_1)$ as a weight factor). In order to be on the conservative side, the error bars for all the parameters have been chosen by taking the largest of these two lines.

The derived value of the radial velocity semi-amplitude K_1 is highly inconsistent with that one of Shafter (1984). It is not easy to explain why his result is so different, as he did not present his analysis in detail. A possible reason might be poor spectral resolution for Shafter’s data ($\approx 10\text{ \AA}$) and as a consequence the wider Gaussians used in the double-Gaussian method.

It is well known that the application of the double Gaussian method to CVs often gives quite uncertain or incorrect results, as the emission lines arising from the disc may suffer several asymmetric distortions. Taking these potential sources of errors into consideration, we believe we could avoid them. In our study of UX UMa, both the obtained values of K_1 are consistent with each other. Though the detected asymmetric emission structure of UX UMa (particularly, the dark spot in the lower-left of the $H\beta$ Doppler map, and the spiral pattern in the $H\alpha$ tomogram) may potentially influence the velocity determination, we hope we could

Table 2. Elements of the radial velocity curves of UX UMa derived from emission lines H α and H β .

Emission line & dataset	K ₁ (km s ⁻¹)	γ -velocity ^a (km s ⁻¹)	φ_0 ^b
H α - Loiano	117 \pm 8	-59 \pm 6	0.037 \pm 0.012
H β - SAO	106 \pm 11	-54 \pm 9	-0.025 \pm 0.020
Adopted Value	113\pm11	-57\pm9	0.020\pm0.020

^a The measured γ -velocities are heliocentric. The mean value was obtained after correction for the solar motion.

^b Phases were calculated according to ephemeris (1).

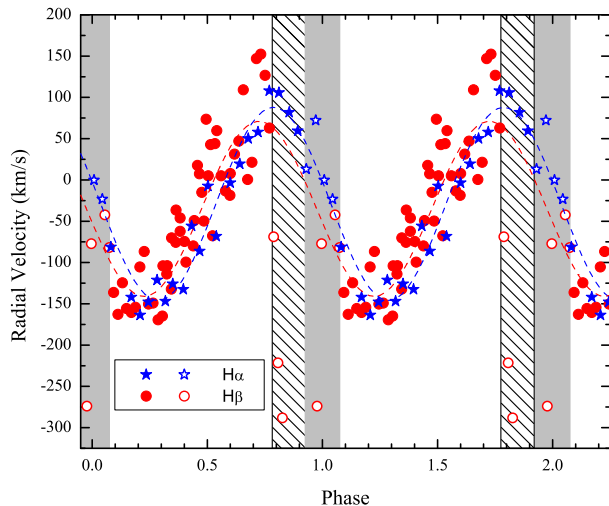


Figure 5. The H α (blue stars) and H β (red circles) radial velocities folded on the orbital period. Two cycles are shown for clarity. The vertical area, shown in gray, marks the eclipsing phase range. The hatched area marks the phase range prior to eclipse, during which the H β emission line was affected by the absorption component. Open symbols indicate data omitted during the fitting procedure.

avoid this as those strong structures are situated well inside of the chosen Gaussian separation. The correct phasing of the radial velocity curve also strengthens our confidence. On the other hand, we cannot exclude the possibility that some other yet-unknown effects may distort our results.

4 DOPPLER TOMOGRAPHY

The orbital variation of the spectral lines profiles indicates a non-uniform structure for the accretion disc. In order to study the emission structure of UX UMa we have used Doppler tomography. Full technical details of the method are given by Marsh & Horne (1988) and Marsh (2001). Examples of the application of Doppler tomography to real data are given by Marsh (2001).

Figures 6–7 show the tomograms of the different spectral lines from the SAO and Loiano sets of observations, computed using the code developed by Spruit (1998). The figures also show trailed spectra in phase space, from which the maps were computed, and their corresponding reconstructed counterparts. As the gradual occultation of the emitting regions during eclipse is not taken into

account, we constrained our data sets by removing eclipse spectra covering the phase ranges $\phi = 0.92$ –1.08.

To assist the interpretation of the Doppler maps, the positions of the WD (lower cross), the center of mass of the binary (middle cross) and the Roche lobe of the secondary star (upper bubble with the cross) are marked. The predicted trajectory of the gas stream and the Keplerian velocity of the disc along the gas stream have also been shown in the form of the lower and upper curves, respectively. The Roche lobe of the secondary and the trajectories have been plotted using the system parameters, derived by Baptista et al. (1995) – an inclination $i = 71^\circ$ and $M_1 = M_2 = 0.47M_\odot$.

The spectral lines in UX UMa (especially He I) require negative values in some parts of the tomogram in order to fit the absorption component of the line. To avoid this, we have followed an approach of Marsh et al (1990). Prior to the reconstruction, we have added a Gaussian of FWHM = 600 km s⁻¹ to the data in order to avoid the need for negative pixel values. We then removed the Gaussian equivalent from the calculated tomogram to produce the final result. This procedure has no effect on the goodness of the fit or entropy when the latter is determined over small scales.

The appearance of all the tomograms from the SAO dataset is extremely unusual. We start to discuss them from the H β emission line as this is the strongest line and it produces a map of the highest quality. Due to the non-double-peaked line profile of H β we did not expect a Doppler map to have an annulus of emission centered on the velocity of the WD, and the observed tomogram does not show it. Instead of this the map displays a very non-uniform distribution of the emission. It appears to be dominated by emission consistent with an origin on the secondary star, from the relatively weak bright-spot located in the region of interaction between the gas stream and the outer edge of the accretion disc, and also from the leading side of the accretion disc (the right side of the tomogram), whose interpretation is ambiguous and will be discussed later.

But the most intriguing and undoubtedly unique feature of UX UMa’s tomogram is a “dark spot” – a compact *absorption* area with FWHM $\lesssim 250$ –300 km s⁻¹, centered on ($V_x \sim -160$ km s⁻¹, $V_y \sim -440$ km s⁻¹) – which is associated with the absorption S-wave in the trailed spectra. This region is situated far from the region of direct interaction between the stream and the disc particles, and from this point of view the location of any structures here is unexpected. However, many NL systems and especially the SW Sex stars show the emission in the lower-left quadrant of the tomogram but, to the best of our knowledge, UX UMa is the only CV that exhibits the absorption here.

The appearance of the H γ and H δ maps is similar to the H β map, though “the dark spot” here is even deeper and more extended in velocity space. The He I Doppler maps also have a similar morphology to the Balmer lines. The main difference between them is a different contribution of the above-mentioned components. So, emission from the secondary star is, at best, very weak whereas the absorption is strong and extended across a wide range of velocities. This reason makes the tomograms look noisy, as the emission component in most He I lines is rather weak and we have had to apply an aggressive intensity scaling for these lines. The dark spot in the different lines is closely spaced on the tomograms, though it is difficult to determine its exact coordinates when it is as extended as in He I $\lambda 4026$ and $\lambda 4471$. However, it seems that the dark spot in He I is slightly shifted along azimuth respectively to the Balmer lines.

The high-excitation emission lines show little variation with time and produce quite noisy tomograms with little details. However, a most prominent contribution of the emission here is from

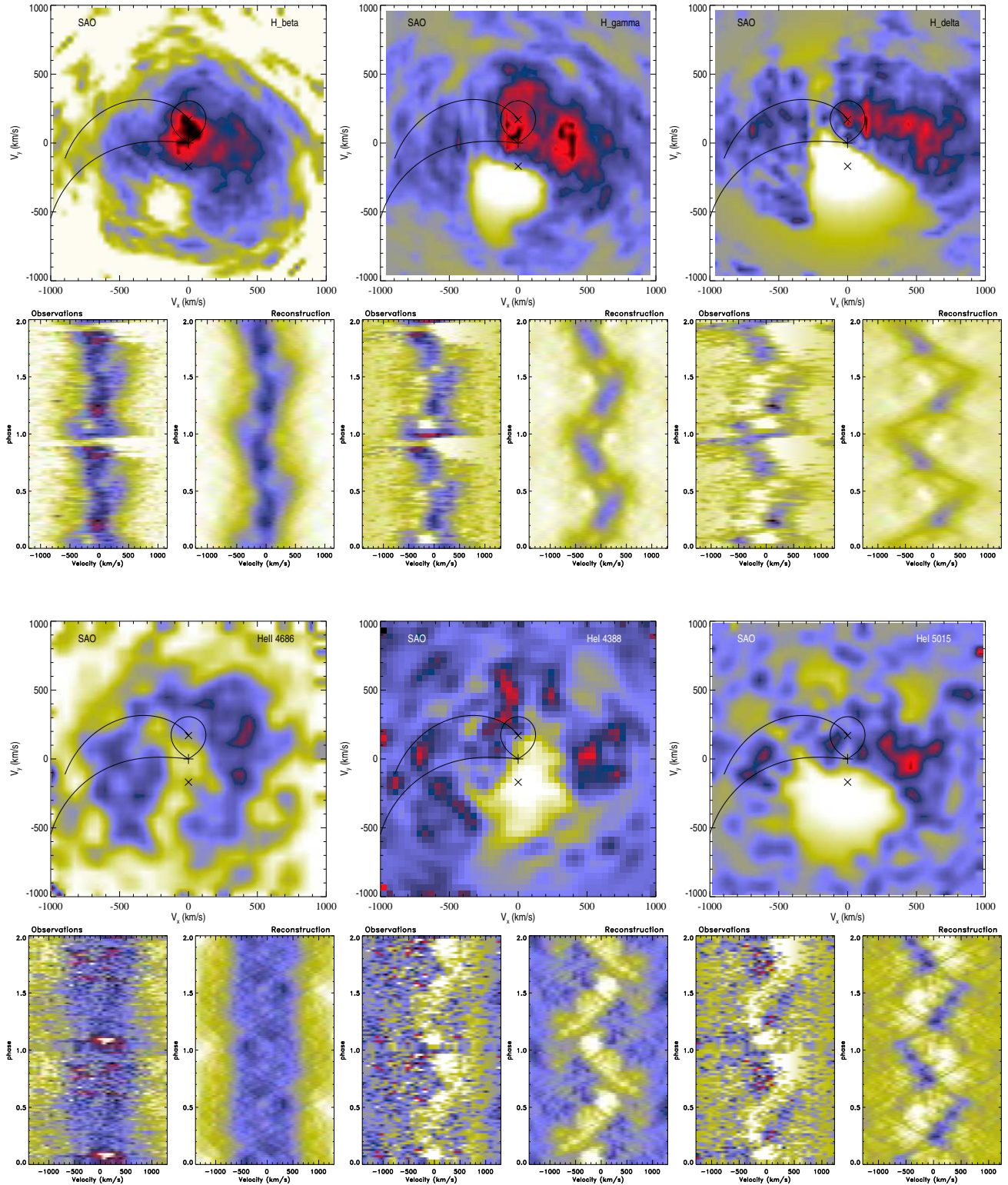


Figure 6. Doppler tomography for the $H\beta$, $H\gamma$ and $H\delta$ emission lines (in the upper half of Figure), and for $He\ II\ \lambda 4686$, $He\ I\ \lambda 4388$ and $He\ I\ \lambda 5015$ (in the bottom half of Figure) from the SAO set of observations. For each line the observed and reconstructed trailed spectra (bottom) and corresponding Doppler maps (top) are shown. Marked on the maps are the positions of the WD (lower cross), the center of mass of the binary (middle cross) and the Roche lobe of the secondary star (upper bubble with the cross). The predicted trajectory of the gas stream and the Keplerian velocity of the disc along the gas stream have also been shown in the form of the lower and upper curves, respectively. The Roche lobe of the secondary and the trajectories have been plotted using the system parameters, derived by Baptista et al. (1995) – an inclination $i = 71^\circ$ and $M_1 = M_2 = 0.47M_\odot$. The flux scale is from white to black.

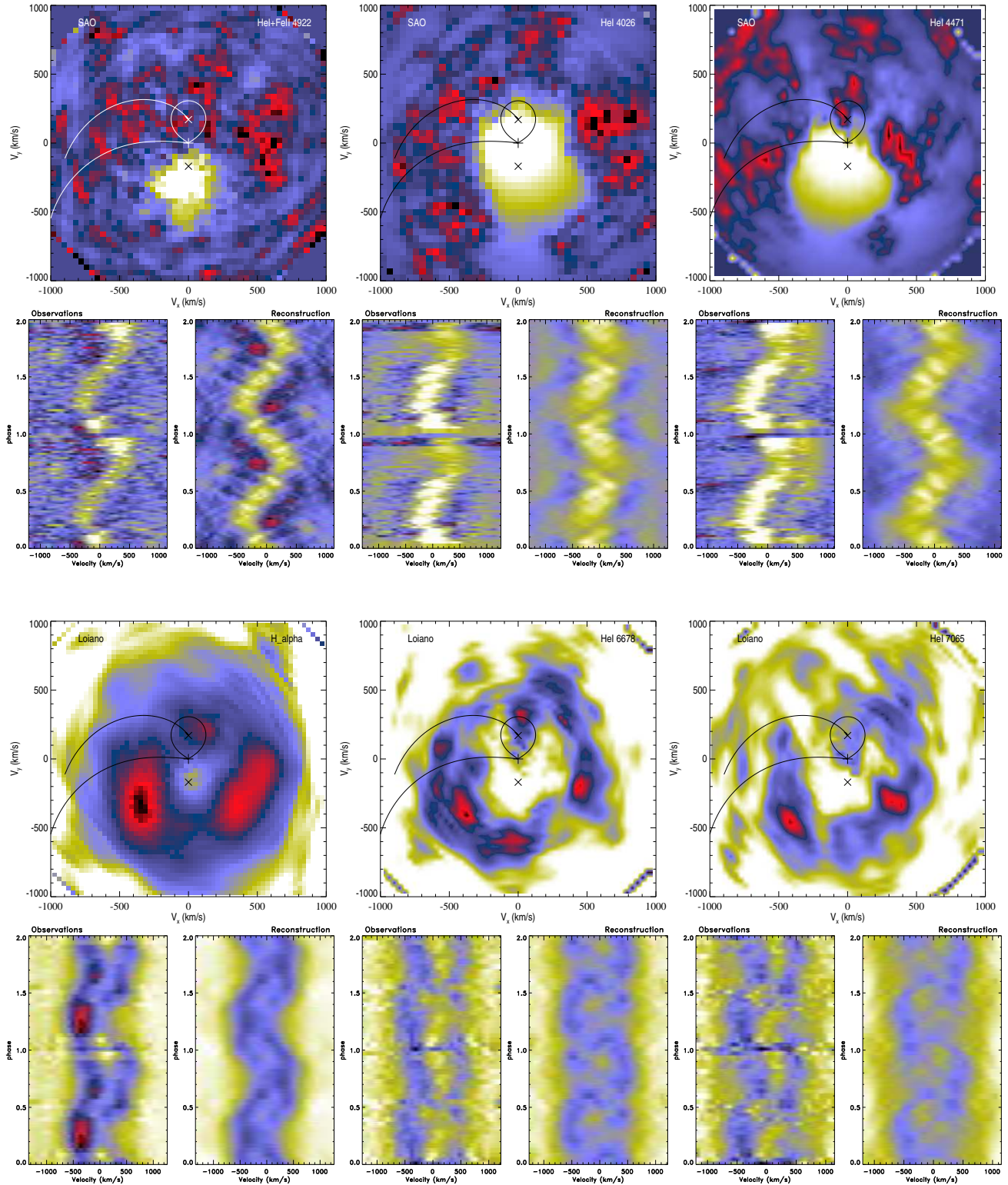


Figure 7. Doppler tomography for the He I $\lambda 4922$, $\lambda 4026$ and $\lambda 4471$ lines from the SAO dataset (in the upper half of Figure), and for the H α , He I $\lambda 6678$ and He I $\lambda 7065$ emission lines from the Loiano set of observations (in the bottom half of Figure). For each line the observed and reconstructed trailed spectra (bottom) and corresponding Doppler maps (top) are shown. Marked on the maps are the positions of the WD (lower cross), the center of mass of the binary (middle cross) and the Roche lobe of the secondary star (upper bubble with the cross). The predicted trajectory of the gas stream and the Keplerian velocity of the disc along the gas stream have also been shown in the form of the lower and upper curves, respectively. The Roche lobe of the secondary and the trajectories have been plotted using the system parameters, derived by Baptista et al. (1995) – an inclination $i = 71^\circ$ and $M_1 = M_2 = 0.47M_\odot$. The flux scale is from white to black.

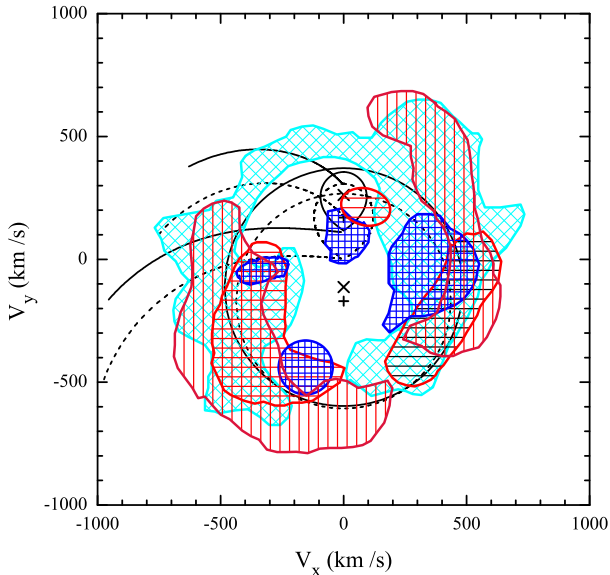


Figure 8. Schematic representation of the essential components of the Doppler maps of UX UMa (Figures 6–7). Different patterns correspond to different emission lines: $H\beta$ (the blue vertical/horizontal cross-hatched area), $He\ II\ \lambda 4686$ (the cyan oblique crosshatched area), $H\alpha$ (the red horizontal hatched area) and the $He\ I$ emission lines from the red wavelength range (the crimson vertical hatched area). Also plotted the positions of the WD, the Roche lobe of the secondary star, and the predicted trajectory of the gas stream and the Keplerian velocity of the disc along the gas stream, using the dynamical solution from this paper (solid lines) and the system parameters, derived by Baptista et al. (1995) (dashed lines). The circles represent the largest radius of the accretion disc determined by tidal limitations.

the quasi-circular structure with a radius of $\sim 500\text{ km s}^{-1}$ centered on the velocity of the WD (see the $He\ II\ \lambda 4686$ map in the bottom half of Fig. 6). Note also that $He\ II\ \lambda 4686$ does not show any emission on the hemisphere of the donor star that faces the WD and boundary layer, and that the circular structure, most likely linked with the accretion disc, has an interruption in the region of the dark spot. There is also enhanced emission from the leading side of the accretion disc.

The red spectra from the Loiano dataset have completely different appearance in comparison with the blue spectra, and as a result the Doppler maps in this wavelength region appear distinctly different (Fig. 7, bottom half). The double-peaked profiles of the $H\alpha$ and $He\ I$ emission lines, attributed to an accretion disc, produce an azimuthally asymmetric annulus of emission centered on the velocity of the WD, revealing a prominent two armed pattern. This pattern resembles the signature generated by spiral structure in the disc, predicted numerically by a number of researchers (Sawada, Matsuda, & Hachisu 1986; Steeghs & Stehle 1999). Comparing the blue and red tomograms, one can also speculate on the same origin of the emission from the leading side of the accretion disc (in the blue spectra) and of one of the arms in the red spectra (Fig. 8). In conclusion, we also note that in contrast to the SAO observations, there is no evidence for both the dark spot and the gas stream/disc impact region emission in the Loiano dataset, while the emission from the area where the secondary star is expected, is weaker and with slightly different velocity coordinates.

Thus, combining all the results above, we conclude that most of the spectral line components in UX UMa appears to originate from four distinct components: the secondary star, the accretion disc with two arch-like structures, the bright spot from the gas

stream/disc impact region, and the dark spot in the lower-left quadrant of the tomograms (Fig. 8). All these components exhibit a different appearance in different spectral lines and in different epochs. A more detailed discussion of the emission structure of UX UMa follows in the next section.

5 THE ACCRETION DISC AND EMISSION/ABSORPTION STRUCTURE OF UX UMa

It is widely accepted that the NL stars experience high mass transfer rates (Puebla, Diaz, & Hubeny 2007; Ballouz & Sion 2009) and their accretion disc is optically thick. As follows from the theoretical calculations, an intrinsic spectrum of such discs should be close to stellar, with absorption Balmer and $He\ I$ lines (Suleimanov 1992; Diaz, Wade, & Hubeny 1996). The irradiation of the standard optically thick disc by the hot central source is not enough to replace the absorption by emission (Kromer, Nagel, & Werner 2007). Emission lines in these systems are believed to originate in a relatively hot extended region above the orbital plane. This extended matter is heated due to the external irradiation by the WD, boundary layer and inner disc. In the inner disc, despite the higher temperatures, the absorption cannot be replaced by emission because the irradiated flux here is insignificant in comparison with the intrinsic flux. Therefore, there are two spatially resolved emitting regions – the inner disc, which has mostly photospheric spectrum with absorption lines, and the outer disc, emitting spectrum with emission lines. Note also that the emission component tends to be more pronounced in high inclined eclipsing systems where the optically thin hot plasma is seen along the disc surface and has more significant optical depth (in comparison with face-on discs, but τ still remains $\lesssim 1$) and therefore larger emission flux, whereas the absorption line core depth decreases with the orbital inclination (Diaz, Wade, & Hubeny 1996; Kromer, Nagel, & Werner 2007). This picture is confirmed by observations of “disc-on” NL stars (TT Ari, V603 Aql) and DNe during outbursts, especially in the UV part of the spectra.

UX UMa is a high inclined eclipsing system and it does not show broad absorptions similar to low inclined TT Ari (Stanishev, Kraicheva, & Genkov 2001). However, it has a steep Balmer decrement outside eclipse phases which suddenly becomes almost flat at mid-eclipse (Fig. 1). This transformation could also be easily explained within the framework of the above-described model: the inner disc with its photospheric spectrum is shielded around mid-eclipse phases by the secondary star, whereas an optically thin line emission region above the orbital plane is still seen and becomes the main contributor to the spectrum.

The oscillator strength for $H\alpha$ is significantly larger than those for the higher members of the Balmer series, thus detection of accretion disc structures is more sensitive in this line. Indeed, usually $H\alpha$ has larger equivalent widths of emission components than the other Balmer lines. Therefore, we can expect that the bright spot and the secondary star in UX UMa should be seen in $H\alpha$ better than in $H\beta$ (similar behaviour is expected for the “blue” and “red” $He\ I$ lines). As such, the changes between the SAO and Loiano spectra most likely testify of time dependence within the system, though part of these changes can be due to different line transfer effects in different lines.

5.1 Dark spot

Whilst the emission in the lower-left quadrant of the tomogram is one of the distinguishing characteristics of the SW Sex-type systems (Hellier 2000), it has also been observed in many CV stars of other types (WZ Sge – Neustroev 1998, BF Eri – Neustroev & Zharikov 2008) and some low mass X-ray binaries (LMXB), (XTE J2123-058 – Hynes et al. 2001, GX9+9 – Cornelisse et al. 2007). Different ideas have been proposed to explain this phenomenon and other probably related observational peculiarities, such as a high-velocity emission S-wave, transient absorption features in the Balmer and He I emission line cores and X-ray/UV dips in the phase range ~ 0.3 – 0.6 . Among these mechanisms invoked are stream overflow (Hellier & Robinson 1994; Hellier 1996), a WD-anchored magnetic field (Williams 1989; Dhillon, Marsh, & Jones 1991), magnetic propeller anchored in the inner disc (Horne 1999), magnetic accretion (Rodríguez-Gil et al. 2001; Hameury & Lasota 2002).

We believe that the compact area of absorption which produced the absorption S-wave in the trailed spectra and the dark spot in the lower-left part of UX UMa’s tomograms, can be explained in the context of the stream-disk overflow model. Numerous theoretical and numerical studies indicate that free flowing gas could pass over the WD and hit the back side of the accretion disc (Lubow & Shu 1976; Lubow 1989; Armitage & Livio 1996, 1998; Hessman 1999). In particular, intensive 3-D smoothed particle hydrodynamics (SPH) simulations show (Kunze, Speith, & Hessman 2001) that a substantial fraction of the stream overflows the outer disc edge and impacts the disc close to the circularisation radius at orbital phase ~ 0.5 . Kunze, Speith, & Hessman (2001) conclude that the presence of substantial quantities of gas above and below the disk plane can cause X-ray absorption in CVs and LMXBs around orbital phase 0.7, if the inclination is at least 65° . We suggest the same might be happening in UX UMa, and the dark spot in the lower-left quadrant of the tomogram, situated around $\varphi \sim 0.6$, might be caused by the deflected stream flow. In case of a rather small disc and the high mass transfer rate or its sudden increase, the overflowing stream might produce a dense lump of matter in the place where it re-enters the disc. This lump and/or the overflowing stream itself can prevent the outer sector of the disc to be irradiated by the hot inner disc that will cause a predominance of absorption over emission here (Fig. 9). As a result we will see a narrow absorption in the spectrum and a dark spot in the tomogram. Considering that the optical depth of the matter in the He I lines is smaller in comparison with the Balmer lines due to the lower helium abundance and the oscillator strengths of the He I lines, it may explain the displacement of the dark spot in the He I lines relative to the Balmer lines.

As the lump will not only occult the outer disc from irradiation but will also shield some part of the disc from the observer, it can also very naturally explain the absorption in the red wings of emission lines observed during the phase range $\varphi \sim 0.78$ – 0.95 . The opacity of the falling stream is most likely anisotropic, increasing along the stream. Thus, around these phases the lump can occult the hottest and brightest innermost part of the accretion disc with the greatest range of the radial velocities, leading to weakening of the emission component in the red wing of spectral lines (Fig. 9).

The supposition that UX UMa had a rather small accretion disc during the SAO observations (smaller than during the Loiano set) is supported by Doppler tomography. All the tomograms from this data set show weak, but clearly seen emission from the bright spot – the region of interaction between the gas stream and the outer

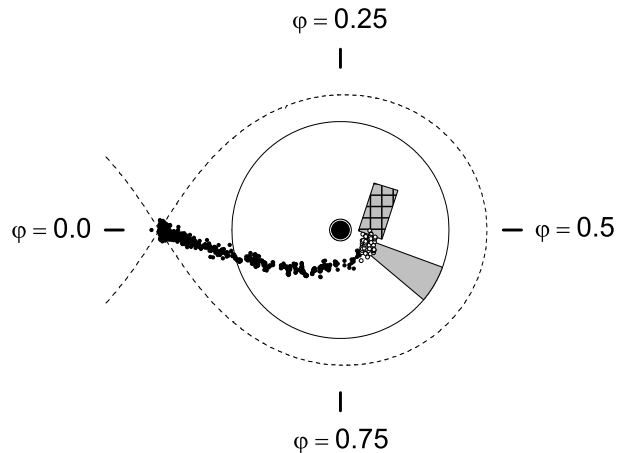


Figure 9. A schematic model of UX UMa. The overflowing stream creates the lump of matter which prevents the outer sector of the disc, shown in gray, to be irradiated by the hot inner disc. The lump and the falling stream also shields a part of the accretion disc from the observer. The cross-hatched area indicates the region of the disc obscured at the orbital phase ~ 0.8 .

edge of the accretion disc. In most of the lines this emission lies over the predicted trajectory of the gas stream, though in a few lines the emission has the Keplerian velocity of the disc along the gas stream. The singularity and difference of UX UMa’s bright spot from those usually observed in CVs consist in its extent. The bright spot in UX UMa appears to be extended over hundreds kilometers per second along the trajectories, which could be due to the matter stream deflecting vertically or penetrating deeply into the disc before finally being deviated.

No such thing has been observed during the Loiano observations. There are no signs of the bright spot lying over either of the trajectories. The accretion disc is large and thick (see the following discussion), the interaction between the stream and the outer part of the disc is less energetic, the lesser part of the stream matter overflows the disc and – as a consequence – there is no dark spot in the lower-left part of the tomograms.

5.2 Spiral pattern

The accretion disc in UX UMa manifests itself as a non-uniform circular structure, with a radius of $\sim 400 \text{ km s}^{-1}$, in the Doppler maps from the Loiano set of observations. The disc emission is not azimuthally symmetrical, but exhibits the two arch-like structures, superposed on the diffuse ring. This pattern resembles the non-axisymmetric features observed in the accretion discs of several DN systems when they were in outburst (IP Peg – Steeghs, Harlaftis, & Horne 1997, U Gem – Groot 2001), and also in a few NLs (V3885 Sgr – Hartley et al. 2005, V1494 Aql – Hachisu, Kato, & Kato 2004). The presence of such structures has been originally interpreted as an observational confirmation for the existence of the tidally induced spiral shocks, predicted by hydrodynamic models of accretion discs in close binaries (Sawada, Matsuda, & Hachisu 1986; Spruit 1987; Steeghs & Stehle 1999; Boffin 2001). Nevertheless, Smak (2001) and Ogilvie (2002) have questioned such interpretation, as it requires the presence of large or unusually hot discs, and proposed alternatives to the spiral shocks to explain the phenomenon. Ogilvie (2002) has shown that some regions of the outer disc would be tidally thickened and may therefore be irradiated by the WD,

boundary layer and/or inner disc. The pattern of thickening would be slightly spiral, but no waves or shocks would be involved in the process. Smak (2001) has wondered if the similar effect should work in CVs with stationary accretion (i.e., novae and NL systems), whose outer radii of the large accretion discs are controlled by tidal effects. He reviewed the collection of Doppler tomograms published by Kaitchuck et al. (1994) and identified similar arch-like structures in tomograms of several NL-systems, including UX UMa. Note, however, that this identification does not exclude the shock origin of these structures but only supports the existence of non-Keplerian flows in the accretion disc of UX UMa.

The appearance of the two armed pattern in UX UMa is a bit different in the $H\alpha$ and He I lines. The structures here are not well-defined spiral arms, though they are possibly connected, overlapping in azimuth ranges where tidal distortions such as spirals are expected. The He I lines are much weaker than $H\alpha$ but the spiral-like structure in their tomograms closely resembles the Doppler maps of those DN systems where spiral structure is basically indisputable. In the $H\alpha$ tomogram, the brightest part of the right arm is placed somewhat lower. Note, that both the theory and the numerical simulations tell us that non-linear effects can significantly modify the appearance of the spiral pattern (e.g. Godon, Livio, & Lubow 1998; Steeghs & Stehle 1999).

Despite the dissimilarity between the red and blue tomograms of UX UMa from our observations, they have (the only) common component – extended bright area from the leading side of the accretion disc. The second, lower-left arm cannot be detected in the blue Balmer and He I tomograms as it is hidden by the dark spot, if exists. However, the He II $\lambda 4686$ map shows some extended emission in the lower-left area (Fig. 8). Furthermore, Kjurkchieva et al. (2006) employed a spiral arm model to explain the observed features of the light curves of UX UMa from their 9-year photometry, and the model reproduced well the observational data. Thus, the spiral-like pattern is apparently a regular structure in the disc of UX UMa.

At present there are arguments in favour and against both models, proposed to explain the spirals (see Morales-Rueda 2004, and references therein). The NL systems with their large, hot and stable accretion discs can be considered as the best systems in which to analyse these structures. Nevertheless, despite the wealth of observations of these stars, and some twenty published Doppler maps, only very few NL systems have shown signs of spiral structure in their discs (V347 Pup – Still, Buckley, & Garlick 1998, V1494 Aql – Hachisu, Kato, & Kato 2004, V3885 Sgr – Hartley et al. 2005). From this point of view UX UMa is an attractive candidate for high time and spectral resolution spectroscopic observations.

5.3 Secondary star

The secondary star manifests itself in the trailed spectrum of $H\beta$ as a narrow sinusoidal emission component, which is mapped onto the inner hemisphere of the secondary's Roche lobe. The emission from this area is clearly seen in all the Balmer Doppler maps (in $H\beta$ this is the strongest emission component), however its distribution over the mass donor is again different in the two data sets. In the SAO spectra the whole donor hemisphere, facing the WD, appeared to be a source of emission, with the emission intensity becoming stronger near the first Lagrangian point. Such distribution almost certainly exclude the possibility of photospheric line emission and the most likely cause of this emission is irradiation by UV-light from the accretion disc, boundary layer or bright spot.

The $H\alpha$ emission from this area in the Loiano spectra is much

weaker. It is slightly shifted in a clockwise direction and apparently concentrates towards poles of the irradiated hemisphere (Fig. 8). The origin of this emission is not so clear and its link with the companion star can be put in doubt². If this emission indeed belongs to the secondary star then the appearance of the $H\alpha$ tomogram suggests irradiation with shielding of the mass donors equatorial regions by the the discs outer rim (Sarna 1990). From this we estimate a height-to-radius ratio (H/R) to be ~ 0.25 (for the system parameters of Baptista et al. 1995). This is an extremely high H/R ratio, at least from a theoretical point of view, although there are some other observations suggesting highish H/R 's (e.g. Mason, Drew, & Knigge 1997 found that the vertical structure of the accretion disc of UX UMa can extend to $H/R \sim 0.36$ above the orbital plane). On the other side, the lack of emission from the secondary star during Loiano observations will mean that something completely blocked the irradiation sources. Otherwise the secondary should be easily seen in $H\alpha$ as it was previously seen in $H\beta$. In this case the H/R ratio can be even greater.

It is interesting to note that there is no evidence for shielding in the SAO tomograms. This means the accretion disc had the smaller H/R ratio at that time. This might have happened if the disc was significantly smaller³. The presence of spiral waves or the tidally thickened regions in the accretion disc during the Loiano run, and only uncertain indications of it during the SAO observations indirectly confirms this idea, as the tidally induced spiral structures require the presence of a large disc.

The detected emission from the secondary star in the Doppler maps allows us to estimate K_2 . The radial velocity of the inner face of the secondary about the centre of mass of the system is lower than the radial velocity of the centre of mass of the secondary, thus a measurement of the velocity of the emission feature from the tomograms will set a lower limit to the radial velocity semi-amplitude K_2 of the secondary. From the Doppler map of $H\beta$ we find $K_2 > 180 \text{ km s}^{-1}$, whereas the $H\alpha$ tomogram increases this limit to $\sim 200 \text{ km s}^{-1}$. Thus, this limit does not contradict with the value of $K_2 = 262 \text{ km s}^{-1}$ obtained by Vande Putte et al. (2003), though the latter appears to be slightly overestimated. Indeed, Vande Putte et al. (2003) obtained K_2 using the far-red absorption lines, which may arise in the back (non-irradiated) side of the secondary. However, this hypothesis requires further study.

6 DISCUSSION

6.1 Long-term variability

The appearance and behaviour of the spectra obtained in 1999 and 2008 indicates that UX UMa may have been in different states during those observations. In 1999 the accretion disc of the system appeared to be smaller than in 2008 and we suggest that it might have been due to the smaller mass transfer rate in 1999. Unfortunately, we are unable to make a conclusion regarding whether one epoch of observations was notably brighter than the other. The absolute flux calibration of our spectroscopy is not completely reliable, and also

² Note, that simulations show that the Maximum Entropy Method applied during the Doppler tomography reconstruction can perhaps be partly responsible for the above effects by blurring/smoothing the compact emission sources (see, e.g. Harlaftis & Marsh 1996)

³ It cannot be excluded also the smaller vertical extension of the irradiation source at that time. However, this is unlikely that such extension can be comparable with the outer disc thickness unless the disc is not small enough.

the spectra were obtained in different wavelength ranges. Bearing in mind that UX UMa's colours can change significantly with time (Dmitrienko 1994), it does not make sense to compare the fluxes of the spectra. Amateur observations also cannot help as they provide us with only sparse data.

However, a variation of the mass-transfer rate in the NL systems is not unusual, and UX UMa is not an exception. Many researchers mentioned UX UMa's peculiar light curves which could be interpreted as being due to a much lower relative luminosity of the hot spot and accordingly to the lower mass-transfer rate. Smak (1994b) noted that the standard and peculiar light curves of UX UMa appear to occur with comparable frequency. Knigge et al. (1998) reported on a fairly substantial increase in the accretion rate in UX UMa by $\gtrsim 50\%$ within three months.

6.2 System parameters

Most of the parameter estimates for UX UMa were found in the past by means of analysis of WD eclipse features in the light curve in the different wavelengths, whereas the value of the radial velocity semi-amplitude K_1 was mostly used in order to support or confirm a photometric solution (Smak 1994a; Baptista et al. 1995). The parameters, derived by Baptista et al. (1995) and commonly adopted in the literature (an inclination $i = 71^\circ$ and $M_1 = M_2 = 0.47M_\odot$) were determined using the UV light curve and the Shafter's value of $K_1 = 160 \text{ km s}^{-1}$.

However, the value of K_2 obtained by Vande Putte et al. (2003), along with our estimates of K_1 and K_2 , immediately refute the Baptista et al.'s parameters. We can determine the parameters of UX UMa using a traditional spectroscopic solution based on the derived radial velocity semi-amplitudes. In order to calculate the masses of the binary, we assume that the semi-amplitudes of the measured radial velocities represent the true orbital motion of the stars. Combining our $K_1 = 113 \pm 11 \text{ km s}^{-1}$ and taking $K_2 = 262 \pm 14 \text{ km s}^{-1}$ from Vande Putte et al. (2003) and P from equation (1), we find the mass ratio $q \equiv M_2/M_1 = K_1/K_2 = 0.43 \pm 0.07$, the masses of each component of the system

$$M_1 \sin^3 i = \frac{PK_2(K_1 + K_2)^2}{2\pi G} = 0.75 \pm 0.20M_\odot, \quad (3)$$

$$M_2 \sin^3 i = \frac{PK_1(K_1 + K_2)^2}{2\pi G} = 0.32 \pm 0.10M_\odot, \quad (4)$$

and the projected binary separation

$$a \sin i = \frac{P(K_1 + K_2)}{2\pi} = 1.46 \pm 0.10R_\odot. \quad (5)$$

The orbital inclination of UX UMa was determined in various papers, ranging from $i = 65^\circ$ to 75° . Using this, we now have the pure dynamical solution for the parameters of UX UMa: $M_1=0.83-1.01 (\pm 0.20) M_\odot$, $M_2=0.36-0.43 (\pm 0.10) M_\odot$, $a=1.51-1.61 R_\odot$, $i=65^\circ-75^\circ$ ($i = 65^\circ$ corresponds to the largest masses and a).

The additional step is to make use of a reasonable assumption that the secondary star fills its Roche lobe. The relative size of the donor star is therefore constrained by Roche geometry and the donor must obey the period-density relation for Roche lobe filling objects (Warner 1995). Using any of the recently obtained empirical and theoretical mass-period relations we obtain the mass for the secondary $0.41-0.45 M_\odot$ (see, for example, Warner 1995; Patterson et al. 2005), which is in a good agreement with the dynamical solution.

During the Loiano observations, the emission lines exhibited double-peaked profiles with the averaged measured peak-to-peak

velocity separation in $H\alpha$ of $\approx 740 \text{ km s}^{-1}$. Smak (1981) has shown that the distance between the peaks in the double-peaked profiles can be used to determine the velocity of the outer rim of the accretion disc V_{out} which in turn depends on the mass M_1 and the radius of the disc. The largest radius of the accretion disc, should it be determined from observations, can further limit the system parameters.

The outer parts of the disc are under the gravitational influence of the secondary star, which prevents the disc from growing larger than R_{max} . This largest radius is determined by tidal limitations. Tidal stress and viscous stress become comparable at this radius and truncate the disc (Warner 1995 and references therein). The largest radius can be estimated by the use of equation (2.61) from Warner (1995), and for the mass ratio $q = 0.43$ we obtain

$$R_{max} = 0.6 a / (1 + q) = 0.42 a = 0.61 R_{L1} \quad (6)$$

where R_{L1} is the distance of the inner Lagrangian point from the WD.

Unfortunately, although the observed spiral-like pattern is an indirect manifestation of the large accretion disc in UX UMa, its estimated size appears to be implausibly large. Based on the obtained system parameters and assuming the Keplerian velocity in the accretion disc, it gives an estimate of the outer radius of the disc to be $R_{out} \approx 0.80 a$, that is even greater than the Roche lobe of the primary.

Should this discrepancy be considered as serious? Generally speaking, yes. Tidal limitations are of fundamental nature whereas the peak separation of a double-peaked emission line is an accurate measure of the velocity of the outer edge of the accretion disc obeying perfect Keplerian rotation.

Nevertheless, there are physical mechanisms which may alter the distance between the peaks. For example, spiral shocks disturb the orderly Keplerian motion in the outermost disk that may result in variability of the inter-peak distance, mostly towards smaller values (Neustroev & Borisov 1998), and this effect is clearly seen in the trailed spectra (Fig. 7, bottom half). Assuming that spiral waves could exist in the accretion disc of UX UMa, we made an attempt to reduce their influence by taking the largest peak separation in $H\alpha$. This approach, however, does not guarantee that this extremal value of $V_{out} \sim 390 \text{ km s}^{-1}$ is close enough to the true velocity of the outer edge of the accretion disc in case of strong shocks, and we indeed found the disc to be very large, almost filling the Roche lobe of the primary ($R_{out}/R_{L1} \sim 0.94$).

Another reason why the distance between the peaks in the double-peaked emission lines can be reduced is a significant amount of emitting matter in the outermost accretion disc with a velocity component perpendicular to the disk plane. Evidences for the presence of winds in nonmagnetic CVs in a state of high mass accretion are unambiguous. Regarding to UX UMa, Knigge & Drew (1997) strongly suggested the presence of a relatively dense and slowly outflowing transition region between the disk photosphere and the fast-moving wind in the system. The presence of strong Balmer emission lines at mid-eclipse during our observations of UX UMa also implies that a part of the line-forming region extends out to distances from the WD. Unfortunately, we can say little about how strong the wind is in the outmost regions of the disc of UX UMa, if it exists at all. Anyway, realization of any of these mechanisms could lead to underestimating of V_{out} .

In conclusion, we have to note that our parameters are not as consistent with Doppler tomography as the parameters of Baptista et al. (1995): the emission from the secondary star overfills the bubble marking the Roche lobe on the tomograms, and also the

stream trajectory is located higher on the maps than the brightest area of the region where we believe the bright-spot is (Fig. 8). As it was mentioned above, the Maximum Entropy Method applied during the Doppler tomography reconstruction can perhaps be partly responsible for the above effects by blurring/smoothing the compact emission sources. Otherwise, it may testify that we still have not constrained the radial velocity semi-amplitudes very reliably in UX UMa. Moreover, it also puts in doubt the independent measurements of K_2 by Vande Putte et al. (2003). Thus, we are now in a situation, when on one side there is a photometric solution which better describes the Doppler maps but definitely cannot be correct, and on the other side is another, spectroscopic solution which we think is closer to the true parameters of UX UMa but does not agree as well with Doppler tomography. One more set of the system parameters obtained by Smak (1994a), is also inconsistent with the former two. Thus, there are still many problems with the parameters of the system, which is considered to be one of the best studied CVs. In order to solve them, new *simultaneous* photometric and spectroscopic observations with high-time resolution will be very useful.

6.3 UX UMa as a SW Sextantis star

During the SAO observations UX UMa showed some of the defining properties of the SW Sex stars, such as single-peaked emission lines with transient absorption features at phase $\sim 0.4 - 0.7$. In this section we summarize these characteristics and compare them with properties of the founding members of the SW Sex sub-class:

(i) UX UMa is the eclipsing system as the founding members of the SW Sex sub-class. Its orbital period of 4.72 h is slightly above but very close to the 3 – 4.5 hr period interval.

(ii) The emission lines in the blue wavelength range are single-peaked as in all the SW Sex stars.

(iii) Significant high excitation spectral features including He II $\lambda 4686$ and Bowen blend emission are typical for the class.

(iv) The transient absorption of the Balmer and He I emission lines reaches its maximum strength at phase ~ 0.58 . The relative intensity of this component increases with the line excitation level. In the He I lines this absorption is a dominating component. The He II $\lambda 4686$ emission line is perhaps not affected by this absorption. Note, that the phase 0.5 absorption in UX UMa is a part of an absorption S-wave. To the best of our knowledge, this is not generally the case in other SW Sex stars. However, we admit that visibility of such S-wave can be governed by some special physical conditions.

(v) The Doppler maps of the SW Sex stars consistently share a common feature: the bulk of Balmer emission is concentrated in the $(-V_x, -V_y)$ quadrant. In this area of UX UMa's tomograms the unique dark spot is located. The dark spot is compact in the Balmer lines and deep and spacious in the He I lines.

(vi) Many SW Sex stars exhibit high-velocity emission S-waves with maximum blueshift near phase ~ 0.5 . This emission is not seen in UX UMa. On the opposite, we have observed the broad absorption depression around the red wings of the Balmer lines just prior to eclipse. This depression is certainly linked with the above-mentioned transient absorption.

(vii) In the eclipsing SW Sex stars the emission-line radial velocity curves show a delay of a 0.1 - 0.2 orbital cycle relative to the motion of the WD. This effect in UX UMa is weak, if exists. Note, however, that Froning, Long, & Knigge (2003) have detected

a phase lag of $\simeq 20^\circ$, compatible with the derived parameters of the radial velocity curves (Table 2).

Thus, many of the characteristics of UX UMa, a prototype of the NL stars and the UX UMa sub-class, are in general accord with the SW Sex systems. Nevertheless, all these features have been observed only in 1999 and almost completely disappeared in 2008. Many symptoms indicate that the system was in different states during those observations. Groot, Rutten, & van Paradijs (2004) proposed that the appearance of a NL system as a UX UMa/RW Tri or SW Sex star seems to be mainly governed by the mass-transfer rate from the secondary at the time of observation, where the SW Sex behaviour becomes more prominent with increasing mass-transfer rate. However, Ballouz & Sion (2009) found little evidence to suggest that the SW Sex stars have higher accretion rates than other NLs above the period gap within the same range of orbital periods. From our observations, we come to a rather contrary conclusion – UX UMa behaved as the SW Sex stars when its mass-transfer rate was perhaps lower than usual. Thus, this hypothesis certainly merits further study.

7 SUMMARY

We have presented an analysis of time-resolved, medium resolution optical spectroscopic observations of the system in the blue (3920–5250 Å) and red (6100–7200 Å) wavelength ranges, that were obtained in April 1999 and March 2008 respectively.

The appearance and behaviour of the spectra indicates that UX UMa has been in different states during those observations. The blue spectra are very complex. They are dominated by strong and broad single-peaked emission lines of hydrogen. The high-excitation lines of He II $\lambda 4686$ and the Bowen blend are quite strong as well. All the lines consist of a mixture of absorption and emission components. Using Doppler tomography we have identified four distinct components of the system: the non-uniform accretion disc, the secondary star, the bright spot from the gas stream/disc impact region, and the unique dark spot in the lower-left quadrant of the tomograms. In the red wavelength range, both the hydrogen ($H\alpha$) and neutral helium (He I $\lambda 6678$ and He I $\lambda 7065$) lines were observed in emission and both exhibited double-peaked profiles. Doppler tomography of these lines reveals spiral structure in the accretion disc, but in contrast to the blue wavelength range, there is no evidence for either the dark spot or the gas stream/disc impact region emission, while the emission from the secondary star is weak.

During the SAO observations UX UMa showed many of the defining properties of the SW Sex stars. However, all these features have been observed only in 1999 and almost completely disappeared in 2008.

We have measured, from the motion of the wings of the $H\alpha$ and $H\beta$ emission lines, the radial velocity semi-amplitude K_1 to be $113 \pm 11 \text{ km s}^{-1}$. We have also restricted the radial velocity semi-amplitude of the secondary star to be $K_2 \gtrsim 200 \text{ km s}^{-1}$. We have used these results to derive the system parameters of UX UMa and found that these estimates are inconsistent with previous values derived by means of analysis of WD eclipse features in the light curve in the different wavelength ranges. It may testify that we still have not constrained the radial velocity semi-amplitudes very reliably in UX UMa.

ACKNOWLEDGMENTS

The authors thank Natalia Neustroeva for help in preparation of the paper. We would like to acknowledge the anonymous referee whose comments have significantly improved this paper. VS thanks DFG for financial support (grant SFB/Transregio 7 Gravitational Wave Astronomy), RBRF (grant 09-02-97013-p-povolzhe-a), and Presidents programme for support of leading science schools (partial support, grant NSH-4224.2008.2).

REFERENCES

- Armitage P. J., Livio M., 1996, *ApJ*, 470, 1024
 Armitage P. J., Livio M., 1998, *ApJ*, 493, 898
 Ballouz R.-L., Sion E. M., 2009, *ApJ*, 697, 1717
 Baptista R., Horne K., Hilditch R. W., Mason K. O., Drew J. E., 1995, *ApJ*, 448, 395
 Beljavsky S., 1933, *Variable Stars*, 4, 196
 Boffin H. M. J., 2001, in *Astrotomography, Indirect Imaging Methods in Observational Astronomy*, ed. H. M. J. Boffin, D. Steeghs, and J. Cuypers, *Lect. Notes Phys.*, 573, 69
 Cornelisse R., Steeghs D., Casares J., Charles P. A., Barnes A. D., Hynes R. I., O'Brien K., 2007, *MNRAS*, 380, 1219
 Dhillon V. S., 1996, in *Evans A., Wood J. H., eds, Cataclysmic Variables and Related Objects*. Kluwer, Dordrecht, p. 3
 Dhillon V. S., Marsh T. R., Jones D. H. P., 1991, *MNRAS*, 252, 342
 Diaz M. P., Wade R. A., Hubeny I., 1996, *ApJ*, 459, 236
 Dmitrienko E. S., 1994, *AstL*, 20, 104
 Froning C. S., Long K. S., Knigge C., 2003, *ApJ*, 584, 433
 Godon P., Livio M., Lubow S., 1998, *MNRAS*, 295, L11
 Groot P. J., 2001, *ApJ*, 551, L89
 Groot P. J., Rutten R. G. M., van Paradijs J., 2004, *A&A*, 417, 283
 Hachisu I., Kato M., Kato T., 2004, *ApJ*, 606, L139
 Hameury J.-M., Lasota J.-P., 2002, *A&A*, 394, 231
 Harlaftis E. T., Marsh T. R., 1996, *A&A*, 308, 97
 Hartley L. E., Murray J. R., Drew J. E., Long K. S., 2005, *MNRAS*, 363, 285
 Hellier C., 1996, *ApJ*, 471, 949
 Hellier C., 2000, *NewAR*, 44, 131
 Hellier C., Robinson E. L., 1994, *ApJ*, 431, L107
 Hessman F. V., 1999, *ApJ*, 510, 867
 Hoard D. W., Szkody P., Froning C. S., Long K. S., Knigge C., 2003, *AJ*, 126, 2473
 Horne K., 1999, in *Hellier C., Mukai K., eds, ASP Conf. Ser. Vol. 157, Annapolis Workshop on Magnetic Cataclysmic Variables*. Astron. Soc. Pac., San Francisco, p. 349
 Hynes R. I., Charles P. A., Haswell C. A., Casares J., Zurita C., Serra-Ricart M., 2001, *MNRAS*, 324, 180
 Kaitchuck R. H., Schlegel E. M., Honeycutt R. K., Horne K., Marsh T. R., White J. C., II, Mansperger C. S., 1994, *ApJS*, 93, 519
 Kjurkchieva D., Marchev D., Khruzina T., Djurašević G., 2006, *Ap&SS*, 306, 217
 Knigge C., Drew J. E., 1997, *ApJ*, 486, 445
 Knigge C., Long K. S., Wade R. A., Baptista R., Horne K., Hubeny I., Rutten R. G. M., 1998, *ApJ*, 499, 414
 Kromer M., Nagel T., Werner K., 2007, *A&A*, 475, 301
 Kukarkin B. V., 1977, *MNRAS*, 180, 5P
 Kunze S., Speith R., Hessman F. V., 2001, *MNRAS*, 322, 499
 La Dous C., 1993, in *Hack M., la Dous C., eds, Cataclysmic Variables and Related Objects*, NASA Monograph Series No. 10, NASA, p. 15
 Linnell A. P., Godon P., Hubeny I., Sion E. M., Szkody P., 2008, *ApJ*, 688, 568
 Lubow S. H., 1989, *ApJ*, 340, 1064
 Lubow S. H., Shu F. H., 1976, *ApJ*, 207, L53
 Marsh T. R., 2001, in *Astrotomography, Indirect Imaging Methods in Observational Astronomy*, ed. H. M. J. Boffin, D. Steeghs, and J. Cuypers, *Lect. Notes Phys.*, 573, 1
 Marsh T. R., Horne K., 1988, *MNRAS*, 235, 269
 Mason K. O., Drew J. E., Knigge C., 1997, *MNRAS*, 290, L23
 Morales-Rueda L., 2004, *AN*, 325, 193
 Neustroev V. V., 1998, *ARep*, 42, 748
 Neustroev V. V., Borisov N. V., 1998, *A&A*, 336, L73
 Neustroev V. V., Zharikov S., 2008, *MNRAS*, 386, 1366
 Ogielvie G. I., 2002, *MNRAS*, 330, 937
 Patterson J., et al., 2005, *PASP*, 117, 1204
 Puebla R. E., Diaz M. P., Hubeny I., 2007, *AJ*, 134, 1923
 Pratt G. W., Mukai K., Hassall B. J. M., Naylor T., Wood J. H., 2004, *MNRAS*, 348, L49
 Rodríguez-Gil P., Casares J., Martínez-Pais I. G., Hakala P., Steeghs D., 2001, *ApJ*, 548, L49
 Rodríguez-Gil P., Schmidtobreick L., Gänsicke B. T., 2007, *MNRAS*, 374, 1359
 Rodríguez-Gil P., et al., 2007, *MNRAS*, 377, 1747
 Rutten R. G. M., Dhillon V. S., Horne K., Kuulkers E., van Paradijs J., 1993, *Nature*, 362, 518
 Rutten R. G. M., Dhillon V. S., Horne K., Kuulkers E., 1994, *A&A*, 283, 441
 Sarna M. J., 1990, *A&A*, 239, 163
 Sawada K., Matsuda T., Hachisu I., 1986, *MNRAS*, 219, 75
 Schneider D. P., Young P., 1980, *ApJ*, 238, 946
 Shafter A. W., 1983, *ApJ*, 267, 222
 Shafter A. W., 1984, *AJ*, 89, 1555
 Shafter A. W., Szkody P., 1984, *ApJ* 276, 305
 Shafter A. W., Szkody P., Thorstensen J. R., 1986, *ApJ*, 308, 765
 Schlegel E. M., Honeycutt R. K., Kaitchuck R. H., 1983, *ApJS*, 53, 397
 Smak J., 1981, *AcA*, 31, 395
 Smak J., 1994a, *AcA*, 44, 59
 Smak J., 1994b, *AcA*, 44, 257
 Smak J. I., 2001, *AcA*, 51, 295
 Spruit H. C., 1987, *A&A*, 184, 173
 Spruit H. C., 1998, preprint (astro-ph/9806141)
 Stanishev V., Kraicheva Z., Genkov V., 2001, *A&A*, 379, 185
 Steeghs D., Harlaftis E. T., Horne K., 1997, *MNRAS*, 290, L28
 Steeghs D., Stehle R., 1999, *MNRAS*, 307, 99
 Still M. D., Buckley D. A. H., Garlick M. A., 1998, *MNRAS*, 299, 545
 Suleimanov V. F., 1992, *SvAL*, 18, 104
 Suleimanov V. F., Neustroev V. V., Borisov N. V., Fioktistova I. S., 2004, *RMxAC*, 20, 270
 Thorstensen J. R., Ringwald F. A., Wade R. A., Schmidt G. D., Norsworthy J. E., 1991, *AJ*, 102, 272
 Vande Putte D., Smith R. C., Hawkins N. A., Martin J. S., 2003, *MNRAS*, 342, 151
 Walker M. F., Herbig G. H., 1954, *ApJ*, 120, 278
 Warner B., 1995, *Cataclysmic Variable Stars* (Cambridge Astrophysics Ser. 28; Cambridge: Cambridge Univ. Press)
 Warner B., Nather R. E., 1972, *MNRAS*, 159, 429
 Warner B., Woudt P. A., 2002, *MNRAS*, 335, 84
 Williams R. E., 1989, *AJ*, 97, 1752

Wood J. H., Naylor T., Marsh T. R., 1995, *MNRAS*, 274, 31

This paper has been typeset from a \TeX / \LaTeX file prepared by the author.

